ARTICLE IN PRESS

Catalysis Today xxx (xxxx) xxx–xxx

Contents lists available at ScienceDirect

Catalysis Today

journal homepage: www.elsevier.com/locate/cattod

CO_2 hydrogenation to methanol over Rh/In_2O_3 catalyst

Jing Wang, Kaihang Sun, Xinyu Jia, Chang-jun Liu*

School of Chemical Engineering and Technology, Tianjin University, Tianjin 300072, China

ARTICLE INFO

Keywords:
Rh
In_2O_3
CO_2
Hydrogenation
Methanol
Oxygen vacancy

ABSTRACT

CO_2 hydrogenation to methanol is of great significance for the emission control and utilization of CO_2. In this work, the Rh/In_2O_3 catalyst with high Rh dispersion was prepared by deposition-precipitation method. The catalyst characterization demonstrates that the highly dispersed Rh species promotes the dissociative adsorption and spillover of hydrogen, which further enhances not only the formation of surface oxygen vacancy of In_2O_3 but also CO_2 adsorption and activation. Enhanced activity was thereby achieved for selective hydrogenation of CO_2 to methanol. A CO_2 conversion of 17.1 % with methanol selectivity of 56.1 %, corresponding to a methanol space time yield (STY) up to 0.5448 $g_{MeOH}\ h^{-1}\ g_{cat}{}^{-1}$, has been obtained under 300 °C, 5 MPa, 76/19/5 of $H_2/CO_2/N_2$ (molar ratio) and 21,000 $cm^3\ h^{-1}\ g^{-1}$ of gas hourly space velocity. Under the same reaction condition, the CO_2 conversion is only 9.4 % with a methanol STY of 0.3402 $g_{MeOH}\ h^{-1}\ g_{cat}{}^{-1}$ over In_2O_3. The methanol selectivity can be even higher than 70 % at the reaction temperatures below 275 °C for Rh/In_2O_3 catalyst.

1. Introduction

CO_2 is one of the major greenhouse gases. With the increasing worldwide concern on CO_2 issue, a great progress has been made in CO_2 capture. The captured CO_2 has been considered as potential feedstock for the synthesis of chemicals and fuels. However, two big challenges remain for how to utilize the captured CO_2 [1]. One is the CO_2-free energy for the conversion of CO_2. The other is the catalyst needed to activate the inert CO_2 molecule and also to convert the activated CO_2 selectively to the desired chemical. For the energy issue, a rapid development of renewable energy has been observed in the recent years. This has made the CO_2 utilization feasible. For the other catalyst challenge, intense research efforts are being made. Many new catalysts have been reported with significantly increasing publications and patents. Some recent reviews have well summarized these publications and patents [2–7].

Among various catalysts being investigated, rhodium (Rh) catalysts have drawn remarkable interests with its extensive applications as homogeneous catalysts for CO_2 conversion. Increasing publications can be found in the literature with the use of heterogeneous Rh catalysts for CO_2 utilization [6,7]. These heterogeneous Rh catalysts have shown high activity for CO_2 reforming [8–11]. They have also shown high activity towards hydrogenation of CO_2 to CO [12–15] and methane [16–22]. Although there were some reported works on the supported Rh catalysts for CO_2 hydrogenation to methanol [7,23–26], the methanol selectivity was not sufficiently high.

On the other hand, CO_2 hydrogenation to methanol (Eq. (1)) has attracted great attentions for CO_2 utilization because methanol is an important intermediate for chemical syntheses. Methanol can be used directly as fuel with easy transportation. The catalyst applied for this reaction normally prefers sufficiently high reaction temperature in order to overcome the kinetic limitation and to achieve high CO_2 conversion. However, CO_2 hydrogenation to methanol has to compete with the endothermic reverse water-gas shift (RWGS) reaction (Eq. (2)) at elevated temperatures. The development of novel catalysts with improved methanol selectivity is immediately needed.

$$CO_2 + 3H_2 \rightarrow CH_3\,OH + H_2O\ \Delta\ H = -49.7\,kJ\,mol^{-1} \tag{1}$$

$$CO_2 + H_2 \rightarrow CO + H_2O\ \Delta\ H = 41.2\,kJ\,mol^{-1} \tag{2}$$

In 2013, In_2O_3 with surface oxygen vacancy was predicted via density functional theoretical (DFT) study by our group to be excellent catalyst for activation and hydrogenation of CO_2 selectively to methanol [27]. It was experimentally confirmed later in 2015 [28]. Further studies confirmed that the combination of In_2O_3 with other oxides (like Ga_2O_3 [29] and ZrO_2 [30–33]) and the addition of metals, like palladium [34,35], nickel [36] and cobalt [37], to In_2O_3 lead to a significantly improved activity. It has been suggested that an intense metal-In_2O_3 interaction exists with the loading of the metal, which causes a big change in the electronic structure of the catalyst and favors the methanol formation. For example, the supported nickel catalyst is normally a highly active catalyst for CO_2 hydrogenation to methane [5–7,38]. However, the methane selectivity is ignorable over the In_2O_3

---

* Corresponding author.
E-mail address: coronacj@tju.edu.cn (C.-j. Liu).

https://doi.org/10.1016/j.cattod.2020.05.020
Received 6 February 2020; Received in revised form 19 April 2020; Accepted 5 May 2020
0920-5861/ © 2020 Elsevier B.V. All rights reserved.

Please cite this article as: Jing Wang, et al., Catalysis Today, https://doi.org/10.1016/j.cattod.2020.05.020

supported Ni catalyst [36]. The methanol selectivity is more than 64 % at temperatures below 275 °C and is even more than 54 % at temperature up to 300 °C over Ni/In_2O_3 [36].

In this work, Rh/In_2O_3 catalyst was prepared and tested for CO_2 hydrogenation to methanol. High methanol selectivity has been achieved. The formation of methane is ignorable. The mechanism for the improved methanol yield of Rh/In_2O_3 has been discussed as well.

2. Experimental

2.1. Catalyst preparation

In_2O_3 was prepared by precipitation method. 5.025 g of indium nitrate $In(NO_3)_3•4H_2O$ (HWRK Chem, 99.99 %) and 7 g $Na_2CO_3•10H_2O$ (Tianjin Kemiou Chemical Reagent, 99 %) were firstly dissolved in 100 mL and 120 mL, respectively. Then the aqueous solution of Na_2CO_3 (0.15 mol/L) was added to the $In(NO)_3$ solution (0.2 mol/L) until pH reaches 7.0 at 80 °C. The mixture was stirred for 3 h at 80 °C. The precipitate was then washed by deionized water several times. Prior to calcination in static air at 450 °C for 3 h, the obtained sample was dried at 80 °C overnight.

RhO_x/In_2O_3 catalyst was prepared by deposition-precipitation method. To make the RhO_x/In_2O_3 catalyst with 1 wt% of Rh loading, 0.0162 g $Rh(NO_3)_3·2H_2O$ (Energy Chemical, 98 %) was firstly dissolved in 50 mL deionized water. 0.495 g as-prepared In_2O_3 was subsequently added into the solution. The resulting slurry was stirred for 1 h at room temperature. Urea (0.3 g) was then added into the slurry. The mixture was subsequently stirred for another 3 h at 80 °C. The precipitate was then washed by deionized water. After that, the obtained sample was freezing dried overnight.

2.2. Catalyst characterization

The catalyst composition was analyzed by using a PerkinElmer Optima 8300 inductively coupled plasma optical emission spectrometer (ICP-OES) equipped with a Teflon sample introduction system. According to the ICP-OES analysis, the Rh loading is 1.07 wt% in RhO_x/In_2O_3, suggesting that Rh was successfully loaded onto In_2O_3 during the catalyst preparation.

The structural properties, including Brunauer-Emmett-Teller (BET) surface area (S_{BET}), total pore volume (V) and average pore diameter (D), were determined by N_2 adsorption/desorption isotherms at 77 K, obtained with an AUTOSORB-1-C instrument (Quantachrome).

The powder X-ray diffraction (PXRD) patterns were recorded on a Rigaku D/MAX-2500 V/PC diffractometer equipped with a Ni-filtered Cu Kα radiation source (40 kV, 200 mA) at a scanning speed of 4°/min over the 2θ range of $10° - 90°$. The phase identification was made by comparison with the X-ray spectrum cards from the Joint Committee on Powder Diffraction Standards (JCPDSs).

Transmission electron microscopy (TEM) measurements were performed on a JEOL JEM-2100 F system equipped with an energy-dispersive X-ray spectrometer (EDX) operated at 200 kV. To do so, the catalyst sample was suspended in ethanol and then dispersed ultrasonically for 30 min. A drop of the suspension was deposited on a copper grid coated with carbon. The suspension was then dried under air.

Hydrogen temperature programed reduction (H_2-TPR) was conducted on a TPDRO 1100 apparatus (Thermo Finnigan, LLC) equipped with a thermal conductivity detector (TCD). The catalyst sample (about 50 mg) was pretreated under flowing argon for 1 h at 200 °C to remove moisture and absorbed water. The sample was then cooled down to room temperature under the flowing Ar. Finally, the sample was heated from room temperature to 700 °C (10 °C/min) under a flow of 10 % H_2/Ar. The consumption of H_2 was measured by the TCD.

Temperature programmed desorption of CO_2 (CO_2-TPD) was carried out to investigate the surface oxygen vacancy of the catalyst. The sample (about 100 mg) was pretreated under flowing argon for 1 h at 300 °C to remove moisture and absorbed water. Then the sample was reduced by 10 % H_2/Ar at 300 °C for 1 h. After that, the sample was cooled down to 50 °C under the same gas stream, followed by CO_2 adsorption at 50 °C for 1 h. After purged with flowing argon to remove physically adsorbed CO_2 at the same temperature, the sample was heated to 700 °C at a rate of 10 °C/min. The products were analyzed using a TCD.

In-situ and *ex-situ* X-ray photoelectron spectroscopy (XPS) analyses were performed on a ThermoFischer ESCALAB 250Xi spectrometer using Al Kα ($h\nu = 1486.6$ eV) radiation. The sample was heated to 300 °C and reduced by H_2 ($H_2/N_2 = 1/9$, mole ratio) for 1 h. The C1 s (284.8 eV) was used as reference for the calibration of binding energies.

2.3. Activity test

The activity tests for CO_2 hydrogenation were conducted in a vertical fixed bed reactor. 0.2 g of the catalyst diluted with 1.0 g of SiC, was loaded in the reactor. Prior to the activity test, the catalyst was purged by N_2 for 0.5 h at room temperature. The catalyst was then pre-reduced by H_2 ($H_2/N_2 = 1/9$, mole ratio) at 300 °C for 1 h under atmospheric pressure. The feed of reactants ($H_2/CO_2/N_2 = 76/19/5$, mole ratio) was then introduced to the reactor at a gaseous hourly space velocity (GHSV) of 21,000 $cm^3\ h^{-1}\ g_{cat}{}^{-1}$ under 5 MPa. The effluent was analyzed by an online gas chromatograph (Agilent 7890D) equipped with a two-column system connected to a flame ionized detector (FID) and a thermal conductivity detector (TCD). All the post-reactor lines and valves were heated to 140 °C to prevent the condensation of methanol.

The CO_2 conversion (X_{CO_2}), the selectivity of product i (S_i) and the space time yield of product i (STY_i) were calculated according to the following equations:

$$X_{CO_2} = \frac{F_{CO_2,in} - F_{CO_2,out}}{F_{CO_2,in}} \times 100\,\%$$

$$S_i = \frac{F_{i,out}}{F_{CO_2,in} - F_{CO_2,out}} \times 100\,\%$$

$$STY_i = \frac{F_{CO_2,in} \times X_{CO_2} \times S_i}{W} \times M_i$$

where F is the molar flow rates of CO_2 or products, M_i is the molar mass of product i, and W is the weight of the catalyst sample.

3. Results and discussion

3.1. Catalyst activity

Fig. 1 shows the profiles of CO_2 conversion, selectivity and STY of methanol and CO with the reaction temperature over In_2O_3 and Rh/In_2O_3 catalysts. Rh/In_2O_3 catalyst shows much higher CO_2 conversion than In_2O_3 in the whole range of temperatures tested. Both catalysts show almost the same methanol selectivity at the reaction temperatures below 275 °C. 100 % methanol selectivity has been obtained at temperatures below 225 °C. The selectivity of methanol is more than 70 % between 225 and 275 °C. When the reaction temperature further increases, the methanol selectivity on Rh/In_2O_3 catalyst is a little lower than In_2O_3. However, at 300 °C, the methanol selectivity is still sufficiently high (56.1 %) with CO_2 conversion of 17.1 % and STY_{MeOH} of 0.5448 $g_{MeOH}\ h^{-1}\ g_{cat}{}^{-1}$ over Rh/In_2O_3 catalyst. This represents a higher methanol selectivity characteristic, compared to the reported Rh catalysts, as shown in Table 1. Carbon monoxide is the main by-product produced from the competitive RWGS reaction (2), which is an endothermic reaction. The higher reaction temperature favors the RWGS reaction. Methane cannot be detected below 275 °C. When the temperature rises to 300 °C, trace methane can be observed. However, the

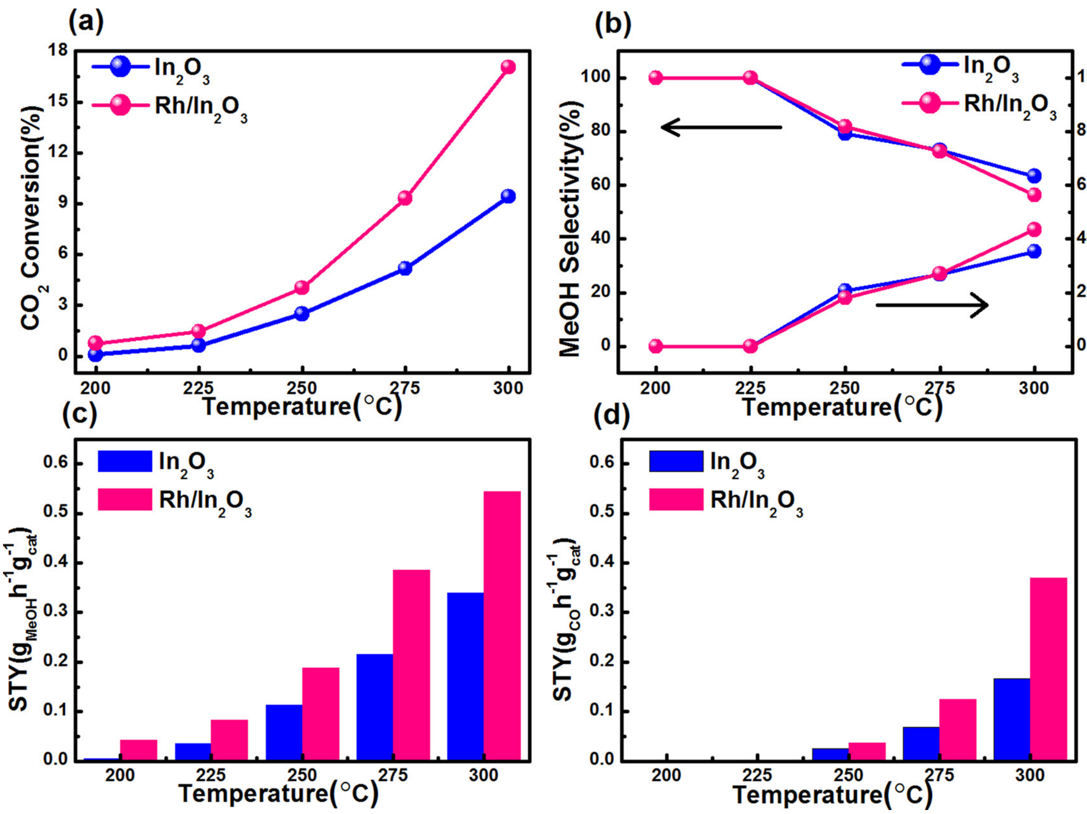

Fig. 1. Catalytic performance of In_2O_3 and Rh/In_2O_3 catalysts: (a) CO_2 conversion, (b) methanol and CO selectivity, (c) methanol STY, (d) CO STY.

peak assigned to methane is too small to be quantitatively measured. The methane formation is therefore ignorable.

3.2. Catalyst characterization

Based on N_2 physisorption measurements at 77 K, the specific BET surface area of In_2O_3 is 72.9 m^2/g, whereas the BET surface area of RhO_x/In_2O_3 is 84.6 m^2/g, which can be attributed to the high Rh dispersion.

The XRD patterns of In_2O_3 and Rh/In_2O_3 catalysts are presented in Fig. 2. Rh/In_2O_3 refers the catalyst after H_2 reduction (H_2/N_2 = 1/9, mole ratio) at 300 °C for 1 h, while In_2O_3-AR and Rh/In_2O_3-AR represent the catalysts after the reaction. Only the peaks of the body-centered cubic In_2O_3 crystalline lattice can be identified for all the catalysts tested. The diffraction peaks at 21.5°, 30.6°, 35.5°, 45.7°, 51.0° and 60.7° belong to the cubic structure of (211), (222), (400), (431), (440) and (622), respectively, according to PDF#06-0416. For the Rh/In_2O_3 catalyst, no characteristic diffraction peaks of rhodium species

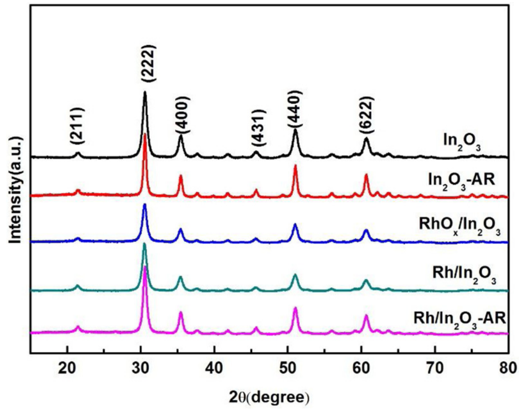

Fig. 2. XRD patterns of In_2O_3 and Rh/In_2O_3 catalysts. (H_2 reduction conditions: 300 °C, H_2/N_2 = 1/9, molar ratio).

Table 1
Comparison of Rh catalysts for CO_2 hydrogenation to methanol.

Catalyst	T (°C)	P (MPa)	GHSV ($cm^3\ g_{cat}^{-1}\ h^{-1}$)	X_{CO2} (%)	S_{MeOH} (%)	STY_{MeOH} ($g_{MeOH}\ g_{cat}^{-1}\ h^{-1}$)	Ref.
Rh/SiO_2	200	5.0	6000	0.5	6.8	0.0008	[12]
RhY	150	3.0	6000	2.8	1.9	0.0011	[16]
Li/RhY	250	3.0	6000	13.1	2.3	0.0065	[23]
$Rh-Fe/TiO_2$	270	2.0	8000	9.2	1.3	0.0066	[24]
Rh/TiO_2	270	2.0	8000	7.9	0.8	0.0036	[24]
$Rh-Co/SiO_2$	260	5.0	6000	15.9	19.9	0.0678	[25]
$Rh-Li/SiO_2$	240	5.0	6000	7.0	5.2	0.0078	[26]
$Rh-Fe/SiO_2$	240	5.0	6000	10.4	16.0	0.0357	[26]
$Rh-Co/SiO_2$	240	5.0	6000	3.7	27.4	0.0217	[26]
$Rh-Sn/SiO_2$	240	5.0	6000	2.8	43.1	0.0259	[26]
Rh/In_2O_3	250	5.0	21,000	4.0	82.0	0.1882	This work
Rh/In_2O_3	275	5.0	21,000	9.3	72.6	0.3853	This work
Rh/In_2O_3	300	5.0	21,000	17.1	56.1	0.5448	This work

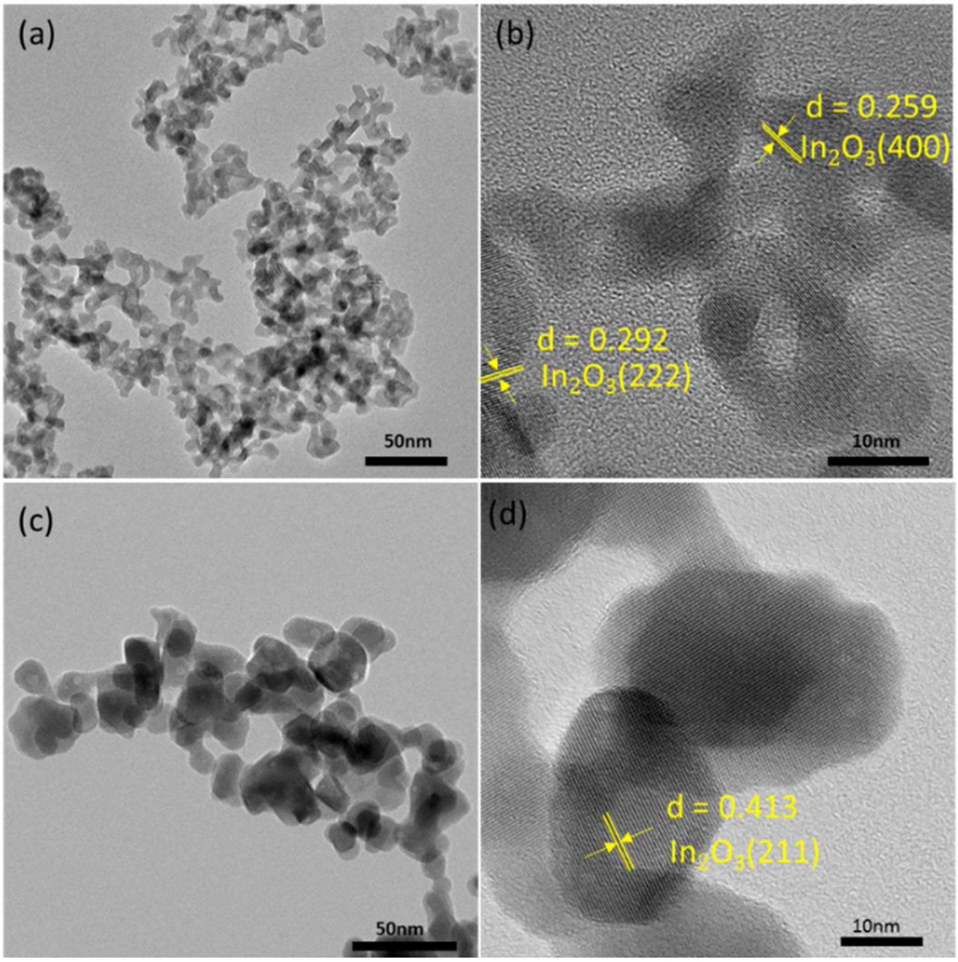

Fig. 3. TEM images: (a) and (b) of fresh In_2O_3; (c) and (d) of In_2O_3-AR.

can be observed. This means ultra-high rhodium dispersion with too small particle size to be measured by XRD analyses. No metallic indium is observed either after the reaction according to the XRD patterns of In_2O_3-AR and Rh/In_2O_3-AR. This suggests In_2O_3 remains the stable crystal structure during the reaction.

Fig. 3 shows the TEM image of In_2O_3 and In_2O_3-AR. Particles of around $10 - 15$ nm are observed in fresh In_2O_3. The lattice fringes with interplanar distance of 0.259 nm and 0.292 nm correspond to the (400) and (222) planes. The (211) plane with interplanar distance of 0.413 nm is also observed. These results are consistent well with the peaks of the cubic In_2O_3 obtained from the XRD analyses. Fig. 4 shows the TEM image of RhO_x/In_2O_3 and Rh/In_2O_3-AR. Rhodium particles cannot be observed in the high resolution TEM analyses. This suggests rhodium is highly dispersed with too small particle size to be identified [39], as discussed in the XRD analyses.

The reducibility of In_2O_3 and RhO_x/In_2O_3 was studied using H_2-TPR, as shown in Fig. 5. For In_2O_3, the broad peaks centered at 150 °C and 300 °C are assigned to the surface reduction of In_2O_3, corresponding to the formation of surface oxygen vacancy. Higher temperature peaks can be attributed to the reduction of bulk In_2O_3 [31,34]. For RhO_x/In_2O_3, H_2-TPR gives an additional peak centered at about 66 °C, which can be assigned to the reduction of RhO_x [40,41]. The presence of supported rhodium nanoparticles makes the peak for the In_2O_3 surface reduction shift to lower temperature at around 125 °C. It also makes the intensity of this peak increase significantly compared with that of pure In_2O_3. This stronger reduction peak at lower temperature indicates more hydrogen is consumed. This means that rhodium can enhance the surface reduction of In_2O_3 and generate more surface oxygen vacancy [34,35].

The CO_2 adsorption and activation were further characterized using CO_2-TPD, as shown in Fig. 6. In addition, it is well known that the surface oxygen vacancy of In_2O_3 can promote CO_2 adsorption and activation so that CO_2 can be also considered as a probe molecular to investigate the properties of surface oxygen vacancy. A single peak at approximate 90 °C for both samples is associated with the physically adsorbed CO_2 [31,34]. The peaks at higher temperature are assigned to the desorption of chemically adsorbed CO_2. For In_2O_3, the peak located at 220 °C is attributed to CO_2 adsorption in the surface oxygen vacancy induced by hydrogen reduction. The peak at about 442 °C is assigned to CO_2 adsorption in the thermally induced oxygen vacancy sites [42]. The presence of Rh species makes the peaks shift to much higher temperature at 263 °C and 542 °C, respectively. It is worth noting that the peaks are also rather stronger, indicating significantly increased surface oxygen vacancy density and enhanced basicity with the load of Rh on In_2O_3. The lower reduction temperature and stronger reduction peak in H_2-TPR curves suggest that rhodium species can enhance the dissociative adsorption and spillover of hydrogen [43,44], which promotes the surface reduction of In_2O_3 and the generation of surface oxygen vacancy, as indicated in CO_2-TPD curves [34,35]. Oxygen vacancy on the In_2O_3 surface then improves the adsorption and activation of CO_2. Consequently, significantly enhanced catalytic activity of CO_2 hydrogenation to methanol is achieved.

XPS analyses were employed to characterize the chemical environment of In, O, and Rh species of the catalysts, as shown in Fig. 7. In 3d core level spectra in Fig. 7(a) presents two peaks at 444.2 and 451.8 eV, which can be attributed to the characteristic spin-orbit split $3d_{5/2}$ and

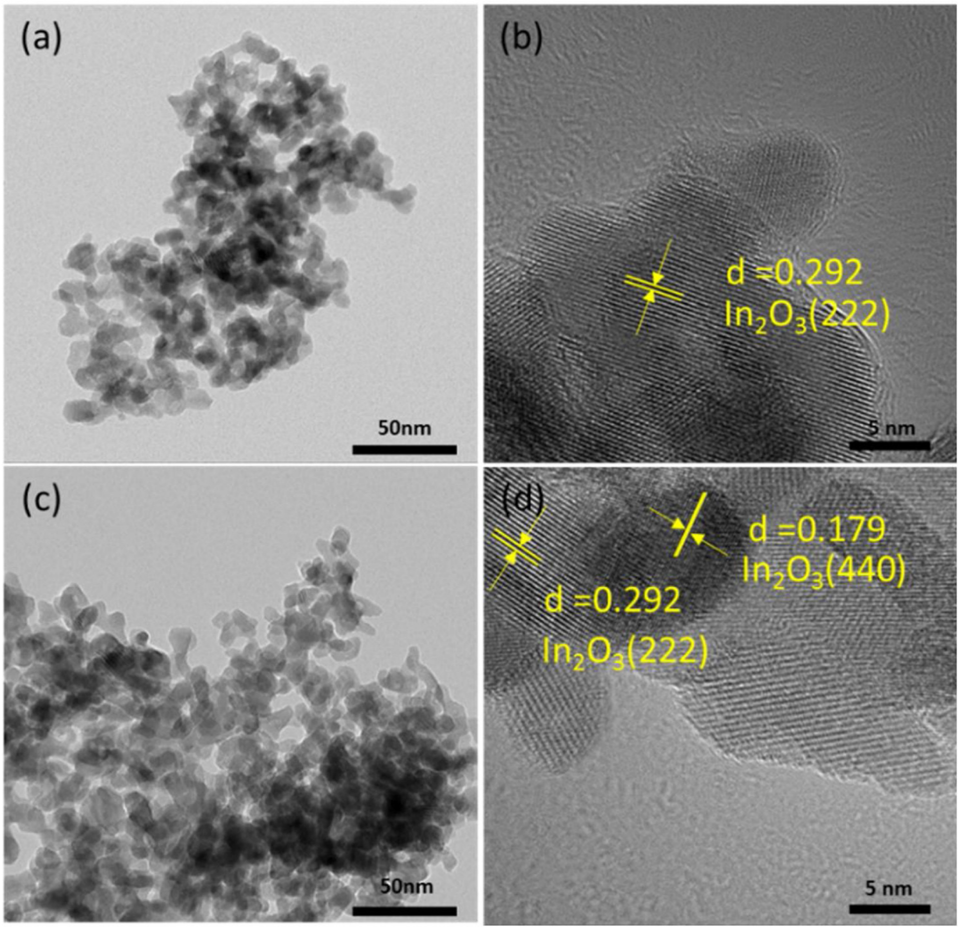

Fig. 4. TEM images: (a) and (b) of fresh RhO_x/In_2O_3; (c) and (d) of Rh/In_2O_3-AR.

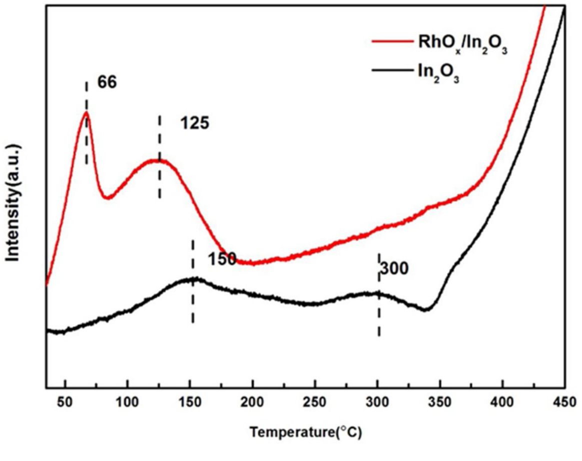

Fig. 5. H_2-TPR profile of In_2O_3 and RhO_x/In_2O_3 catalysts.

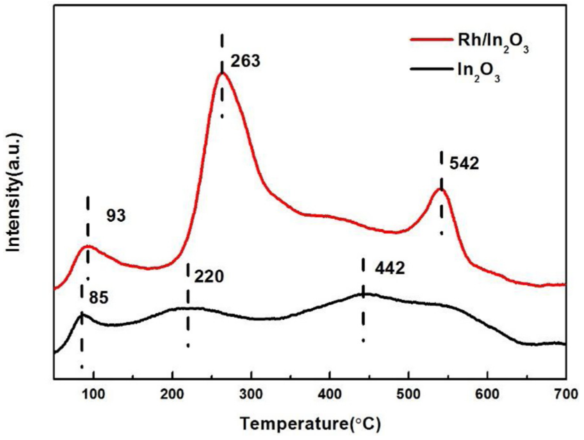

Fig. 6. CO_2-TPD profile of In_2O_3 and Rh/In_2O_3 catalysts.

$3d_{3/2}$, respectively. This indicates the indium valence is mainly +3 for both In_2O_3 and Rh/In_2O_3 catalysts [45].

The O 1s core level spectra are shown in Fig. 7(b). Indeed, the O 1s peak can be deconvoluted into two distinct peaks. The peak at about 529.8 eV corresponds to oxygen in In-O-In ($O_{lattice}$), and the peak at 531.0 eV is commonly attributed to the presence of surface oxygen vacancy ($O_{vacancy}$) [45–47]. $C_{O\text{-vacancy}}$ was used to estimate the relative molar fraction of surface oxygen vacancy ($C_{O\text{-vacancy}} = A_{O\text{-vacancy}}/(A_{O\text{-vacancy}} + A_{O\text{-lattice}})$). $C_{O\text{-vacancy}}$ is 20 % for In_2O_3 and 30 % for Rh/In_2O_3 catalyst. The extra surface oxygen vacancy on Rh/In_2O_3 catalyst is believed to contribute to the superior performance of the catalyst.

To characterize the chemical environment of Rh under hydrogen reduction, *in-situ* XPS spectra were recorded for both fresh and *in-situ* treated catalyst under H_2 (H_2/N_2 = 1/9, mole ratio) at 300 °C for 1 h. The Rh $3d_{5/2}$ peak at 307.3 eV is assigned to Rh^o, while the peak at 309.5 eV is for Rh^{3+} [39,48,49]. In addition, the peaks at higher binding energies are attributed to Rh $3d_{3/2}$. The position of the Rh $3d_{5/2}$ peak for the fresh catalysts is 309.5 eV, confirming that the rhodium valence is mainly +3. After the H_2 treatment, most of rhodium is detected as the form of Rh^o, which is confirmed by the binding energy of 307.3 eV. Herein, Rh^o serves as the active site for dissociative adsorption of H_2, providing sufficient active H atoms for the formation of

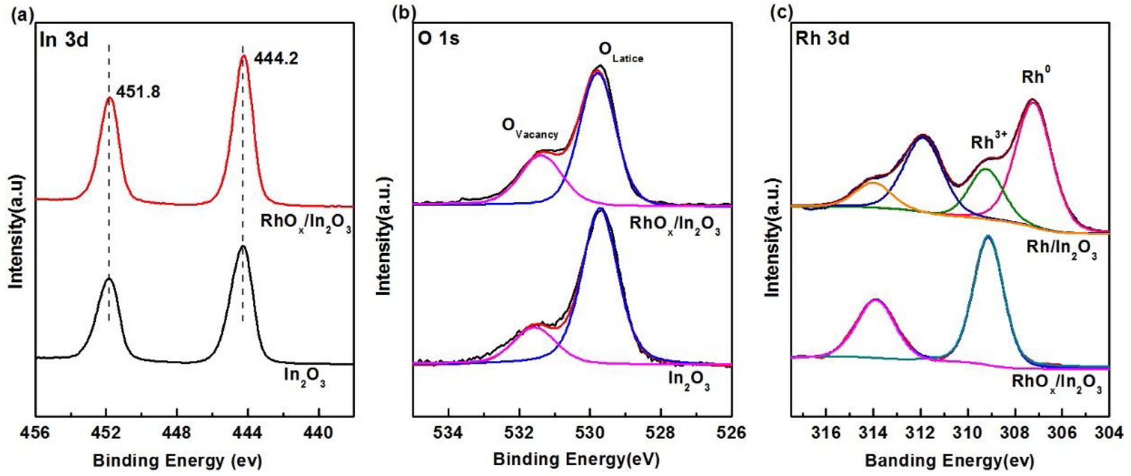

Fig. 7. *In-situ* and *ex-situ* XPS spectra of In_2O_3 and RhO_x/In_2O_3 catalysts: (a) In 3d spectra of *ex-situ* XPS; (b) O 1s spectra of *ex-situ* XPS; (c) Rh 3d spectra of *in-situ* XPS.

surface oxygen vacancy and CO_2 hydrogenation.

4. Conclusions

In this work, Rh/In_2O_3 catalyst with high Rh dispersion was prepared by deposition-precipitation method. The obtained catalyst was confirmed to be highly active for CO_2 hydrogenation with high methanol selectivity, which is 100 % at the reaction temperatures below 225 °C, more than 70 % at temperatures below 275 °C and up to 56 % at 300 °C. The achieved methanol selectivity is higher than the reported Rh catalysts, supported by other oxides. CO is the main by-product produced from the competitive RWGS reaction. The formation of methane is ignorable. The catalyst characterization demonstrates that the highly dispersed Rh species enhance the hydrogen dissociative adsorption and hydrogen spillover, which further promotes the formation of surface oxygen vacancy of In_2O_3. The increased surface oxygen vacancy enhances the adsorption and activation of CO_2 and stabilizes intermediates for synthesis of methanol.

Author statement

Jing Wang and Chang-jun Liu conceived and designed the experiments. Jing Wang prepared the catalysts. Jing Wang, Kaihang Sun and Xinyu Jia carried out the experiments of CO_2 hydrogenation and catalyst characterization. Jing Wang, Kaihang Sun, Xinyu Jia and Chang-jun Liu co-wrote the manuscript. Chang-jun Liu supervised the project. All authors discussed the results and commented on the manuscript.

Declaration of Competing Interest

The authors declare that they have no known competing financial interests or personal relationships that could have appeared to influence the work reported in this paper.

Acknowledgment

This work was supported by the National Natural Science Foundation of China (21536008 and 21621004).

References

[1] C.-J. Liu, Greenh. Gases Sci. Technol. 2 (2012) 75–76.
[2] X. Su, X. Yang, Y. Huang, B. Liu, T. Zhang, Acc. Chem. Res. 52 (2019) 656–664.
[3] S. Liu, H. Yang, X. Su, J. Ding, Q. Mao, Y. Huang, T. Zhang, B. Liu, J. Energy Chem. 36 (2019) 95–105.
[4] T. Zhao, G. Feng, W. Chen, Y. Song, X. Dong, G. Li, H. Zhang, W. Wei, Chin. J. Catal 40 (2019) 1421–1437.
[5] X. Jiang, X. Nie, X. Guo, C. Song, J.G. Chen, Chem. Rev. (2020), https://doi.org/10.1021/acs.chemrev.9b00723.
[6] S. Kattel, P. Liu, J.G. Chen, J. Am. Chem. Soc. 139 (2017) 9739–9754.
[7] A. Erdőhelyi, Catalysts 10 (2020) 155.
[8] Z.-J. Wang, Y. Zhao, L. Cui, H. Du, P. Yao, C.-J. Liu, Green Chem. 9 (2007) 554–559.
[9] I.V. Yentekakis, G. Goula, M. Hatzisymeon, I. Betsi–Argyropoulou, G. Botzolaki, K. Kousi, D.I. Kondarides, M.J. Taylor, C.M.A. Parlett, A. Osatiashtiani, G. Kyriakou, J.P. Holgado, R.M. Lambert, Appl. Catal. B: Environ. 243 (2019) 490–501.
[10] C. Dang, S. Wu, G. Yang, Y. Cao, H. Wang, F. Peng, H. Yu, J. Energy Chem. 43 (2020) 90–97.
[11] S. Praserthdam, P.B. Balbuena, Catal. Today 312 (2018) 23–34.
[12] H. Kusama, K.K. Bando, K. Okabe, H. Arakawa, Appl. Catal. A: Gen. 205 (2001) 285–294.
[13] R. Büchel, A. Baiker, S.E. Pratsinis, Appl. Catal. A: Gen. 477 (2014) 93–101.
[14] D. Heyl, U. Rodemerck, U. Bentrup, ACS Catal. 6 (2016) 6275–6284.
[15] J.C. Matsubu, V.N. Yang, P. Christopher, J. Am. Chem. Soc. 137 (2015) 3076–3084.
[16] K.K. Bando, K. Soga, K. Kunimori, N. Ichikuni, K. Okabe, H. Kusama, K. Sayama, H. Arakawa, Appl. Catal. A: Gen. 173 (1998) 47–60.
[17] A. Beuls, C. Swalus, M. Jacquemin, G. Heyen, A. Karelovic, P. Ruiz, Appl. Catal. B: Environ. 113–114 (2012) 2–10.
[18] C. De Leitenburg, A. Trovarelli, J. Catal. 156 (1995) 171–174.
[19] F. Solymosi, A. Erdöhelyi, Stud. Surf. Sci. Catal. 7 (1981) 1448–1449.
[20] P. Reyes, I. Concha, G. Pecchi, J.L.G. Fierro, J. Mol. Catal. A: Chem. 129 (1998) 269–278.
[21] N.M. Martin, F. Hemmingsson, A. Schaefer, M. Ek, L.R. Merte, U. Hejral, J. Gustafson, M. Skoglundh, A.C. Dippel, O. Gutowski, M. Bauer, P.A. Carlsson, Catal. Sci. Technol. 9 (2019) 1644–1653.
[22] J.B. Branco, P.E. Brito, A.C. Ferreira, Chem. Eng. J. 380 (2020) 122465.
[23] K.K. Bando, K. Soga, K. Kunimori, H. Arakawa, Appl. Catal. A: Gen. 175 (1998) 67–81.
[24] M.R. Gogate, R.J. Davis, Catal. Commun. 11 (2010) 901–906.
[25] H. Kusama, K. Okabe, K. Sayama, H. Arakawa, Appl. Organomet. Chem. 14 (2000) 836–840.
[26] H. Kusama, K. Okabe, K. Sayama, H. Arakawa, Catal. Today 28 (1996) 261–266.
[27] J. Ye, C. Liu, D. Mei, Q. Ge, ACS Catal. 3 (2013) 1296–1306.
[28] K. Sun, Z. Fan, J. Ye, J. Yan, Q. Ge, Y. Li, W. He, W. Yang, C.-J. Liu, J. CO2 Util. 12 (2015) 1–6.
[29] N. Akkharaphatthawon, N. Chanlek, C.K. Cheng, M. Chareonpanich, J. Limtrakul, T. Witoon, Appl. Surf. Sci. 489 (2019) 278–286.
[30] T. Chen, C. Cao, T. Chen, X. Ding, H. Huang, L. Shen, X. Cao, M. Zhu, J. Xu, J. Gao, Y. Han, ACS Catal. 9 (2019) 8785–8797.
[31] O. Martin, A.J. Martín, C. Mondelli, S. Mitchell, T.F. Segawa, R. Hauert, C. Drouilly, D. Curulla–Ferré, J. Pérez–Ramírez, Angew. Chem. Int. Ed. 55 (2016) 6261–6265.
[32] M. Zhang, M. Dou, Y. Yu, Appl. Surf. Sci. 433 (2018) 780–789.
[33] M. Dou, M. Zhang, Y. Chen, Y. Yu, Surf. Sci. 672–673 (2018) 7–12.
[34] N. Rui, Z. Wang, K. Sun, J. Ye, Q. Ge, C.-J. Liu, Appl. Catal. B: Environ. 218 (2017) 488–497.
[35] M.S. Frei, C. Mondelli, R. García–Muelas, K.S. Kley, B. Puértolas, N. López, O.V. Safonova, J.A. Stewart, D.C. Ferré, J. Pérez–Ramírez, Nat. Commun. 10 (2019) 3377.
[36] X. Jia, K. Sun, J. Wang, C. Shen, C. Liu, J. Energy Chem. 50 (2020) 409–415.
[37] A. Bavykina, I. Yarulina, A.J. Al Abdulghani, L. Gevers, M.N. Hedhili, X. Miao, A.R. Galilea, A. Pustovarenko, A. Dikhtiarenko, A. Cadiau, A. Aguilar–Tapia, J.L. Hazemann, S.M. Kozlov, S. Oud–Chikh, L. Cavallo, J. Gascon, ACS Catal. 9 (2019) 6910–6918.
[38] X. Jia, X. Zhang, N. Rui, X. Hu, C.-J. Liu, Appl. Catal. B: Environ. 244 (2019) 159–169.
[39] A. Bueno–López, I. Such–Basáñez, C. Salinas–Martínez de Lecea, J. Catal. 244

(2006) 102–112.
[40] G. Wang, R. Luo, C. Yang, J. Song, C. Xiong, H. Tian, Z.J. Zhao, R. Mu, J. Gong, Sci. China Chem. 62 (2019) 1710–1719.
[41] Q. Zhang, C. Xu, H. Yin, S. Zhou, ACS Omega 4 (2019) 20829–20837.
[42] L. Wang, J. Cai, Y. Xie, J. Guo, L. Xu, S. Yu, X. Zheng, J. Ye, J. Zhu, L. Zhang, S. Liang, L. Wang, IScience 16 (2019) 390–398.
[43] R.E. Ambrusi, M.E. Pronsato, Appl. Surf. Sci. 464 (2019) 243–254.
[44] V.K. Markova, G.N. Vayssilov, N. Rösch, J. Phys. Chem. C 119 (2015) 1121–1129.
[45] C. Janowitz, V. Scherer, M. Mohamed, A. Krapf, H. Dwelk, R. Manzke, Z. Galazka, R. Uecker, K. Irmscher, R. Fornari, M. Michling, D. Schmeißer, J.R. Weber, J.B. Varley, C.G. Van De Walle, New J. Phys. 13 (2011) 85014.
[46] W.C. Chang, C.H. Kuo, C.C. Juan, P.J. Lee, Y.L. Chueh, S.J. Lin, Nanoscale Res. Lett. 7 (2012) 684.
[47] L.B. Hoch, L. He, Q. Qiao, K. Liao, L.M. Reyes, Y. Zhu, G.A. Ozin, Chem. Mater. 28 (2016) 4160–4168.
[48] J. Soria, A. Martinez–Arias, J.L.G. Fierro, J.C. Conesa, Vacuum 46 (1995) 1201–1204.
[49] C.P. Hwang, C.T. Yeh, Q. Zhu, Catal. Today 51 (1999) 93–101.